

Article

Exploring the Effect of NiO Addition to $\text{La}_{0.99}\text{Ca}_{0.01}\text{NbO}_4$ Proton-Conducting Ceramic Oxides

Kaili Yuan ^{1,†}, Xuehua Liu ^{1,*} and Lei Bi ²

¹ Institute of Materials for Energy and Environment, College of Materials Science and Engineering, Qingdao University, Ningxia Road No. 308, Qingdao 266071, China; 2018025338@qdu.edu.cn

² School of Resource Environment and Safety Engineering, University of South China, Hengyang 421001, China; lei.bi@usc.edu.cn or bilei81@gmail.com

* Correspondence: liuxuehua@qdu.edu.cn

† These authors contributed equally to this paper.

Abstract: To improve the performance and overcome the processing difficulties of $\text{La}_{0.99}\text{Ca}_{0.01}\text{NbO}_4$ proton-conducting ceramic oxide, external and internal strategies were used, respectively, to modify $\text{La}_{0.99}\text{Ca}_{0.01}\text{NbO}_4$ with NiO. The external strategy refers to the use of the NiO as a sintering aid. The NiO was added to the synthesized $\text{La}_{0.99}\text{Ca}_{0.01}\text{NbO}_4$ powder as a secondary phase, which is the traditional way of using the NiO sintering aid. The internal strategy refers to the use of NiO as a dopant for the $\text{La}_{0.99}\text{Ca}_{0.01}\text{NbO}_4$. Both strategies improve the sinterability and conductivity, but the effect of internal doping is more significant in enhancing both grain growth and conductivity, making it more desirable for practical applications. Subsequently, the influences of different concentrations of NiO were compared to explore the optimal ratio of the NiO as the dopant. It was found that the sample with 1 or 2 wt.% NiO had similar performance, while with 5 wt.%, NiO doping content hampered the grain growth. In addition, the inhomogeneous distribution of the element in the high-NiO content sample was found to be detrimental to the electrochemical performance, suggesting that the moderate doping strategy is suitable for $\text{La}_{0.99}\text{Ca}_{0.01}\text{NbO}_4$ proton-conducting electrolyte with improved performance. Furthermore, first-principle calculations indicate the origin of the enhanced performance of the internally modified sample, as it lowers both oxygen formation energy and hydration energy compared with the un-modified one, facilitating proton migration.

Keywords: proton-conducting oxide; LaNbO_4 ; NiO; sintering; theoretical calculations



Citation: Yuan, K.; Liu, X.; Bi, L. Exploring the Effect of NiO Addition to $\text{La}_{0.99}\text{Ca}_{0.01}\text{NbO}_4$ Proton-Conducting Ceramic Oxides. *Coatings* **2021**, *11*, 562. <https://doi.org/10.3390/coatings11050562>

Academic Editor: Narottam P. Bansal

Received: 6 March 2021

Accepted: 5 May 2021

Published: 11 May 2021

Publisher's Note: MDPI stays neutral with regard to jurisdictional claims in published maps and institutional affiliations.



Copyright: © 2021 by the authors. Licensee MDPI, Basel, Switzerland. This article is an open access article distributed under the terms and conditions of the Creative Commons Attribution (CC BY) license (<https://creativecommons.org/licenses/by/4.0/>).

1. Introduction

Solid oxide fuel cells (SOFCs) can now be divided into two types depending on the properties of the electrolyte, including oxygen-ion conducting solid oxide fuel cells [1] and proton-conducting solid oxide fuel cells [2]. Classical SOFCs (oxygen-ion conducting electrolyte) require high working temperatures ($>700\text{ }^\circ\text{C}$), which results in many problems, such as electrode sintering, diffusion at the interface, and difficulty in the preparation of seals and interconnection [3]. At the same time, classical SOFCs produce water at the anode side (fuel side), which would dilute the fuel and reduce fuel efficiency. Furthermore, H_2O is likely to oxidize the anode under high loads. In comparison, proton-conducting SOFCs would permit a reduction in working temperatures due to the lower activation energy for proton migration than that for oxygen-ions [4,5].

Meanwhile, water is formed at the cathode side, so the fuel is not diluted, and the anode avoids the danger of being oxidized even at high current conditions [6]. Consequently, proton-conducting SOFCs are currently a popular topic in the field of SOFCs [7,8].

The current state-of-the-art materials are acceptor-doped BaCeO_3 and BaZrO_3 [9]. Although BaCeO_3 -based material has excellent protonic conductivity in the order of $10^{-2}\text{ S}\cdot\text{cm}^{-1}$ ($600\text{ }^\circ\text{C}$), it tends to be vulnerable in the acidic gas environment, such as CO_2 and H_2O [10]. In contrast, BaZrO_3 has excellent chemical stability but requires a high

sintering temperature and exhibits high grain boundary resistance [11]. These materials both have their own merits and limitations, so either their properties must be enhanced or new electrolytes must be found. Among all the new types of proton-conducting oxides, LaNbO_4 (LNO), which is reported to show pure protonic conductivity below 800 °C under wet reducing conditions, is proposed. Without involving the Ba element, LaNbO_4 has excellent chemical stability over the whole testing temperature range, providing an advantage in practical application. Although the motivation of developing LaNbO_4 -based proton conductors is to eradicate Ba as the main element for improved chemical stability, the relatively low conductivity of doped LaNbO_4 hinders its applications. It has been found that the solubility limit of the conventional dopant in LaNbO_4 at the La site is less than 1% [12]. The highest proton conductivity was achieved for Ca-doped LNO, reaching approximately $10^{-3} \text{ S}\cdot\text{cm}^{-1}$ at 800 °C [13]. In spite of the low conductivity, several works have indicated that the LNO-based cells could reach some fuel cell performance by properly tailoring the electrode and reducing the thickness of the dense electrolyte. Fuel cells with $\text{La}_{0.995}\text{Sr}_{0.005}\text{NbO}_4$ electrolyte (thickness $\sim 30 \mu\text{m}$) showed a maximum output power of $1.35 \text{ mW}\cdot\text{cm}^{-2}$ at 800 °C [14]. By tailoring the anode, fuel cells based on LNO electrolyte film deposited on LNO-NiO anodes showed a peak output power of $24 \text{ mW}\cdot\text{cm}^{-2}$ at 750 °C [15]. As the electrolyte material, the LaNbO_4 has to be sintered densely for utilization. Although the sintering ability of LaNbO_4 -based oxides is not as low as that of BaZrO_3 , high sintering temperatures are still needed (such as 1500 °C) for achieving the dense LaNbO_4 membrane [16]. It is reasonable to assume that the conductivity of the sample could be improved if the grain growth of the LaNbO_4 sample could be further enhanced, which reduces the grain boundary resistance [17]. The use of dopant could be a feasible approach to improve the sinterability of the samples, as it was applied before for other proton-conducting oxides [18]. However, the investigation of dopants for LaNbO_4 is scarce to date.

In this study, NiO was used as the dopant for LaNbO_4 , and different strategies were used to explore the best way of using NiO as the dopant. Furthermore, the optimal NiO content was investigated, with the analysis of the electrochemical performance of the samples to explore the factors restricting the conductivity of LaNbO_4 with the use of an NiO dopant.

2. Materials and Methods

The $\text{La}_{0.99}\text{Ca}_{0.01}\text{NbO}_4$ (LCNO) powder was synthesized via a traditional solid-state reaction route. Briefly, the mixture of 1.61 g La_2O_3 (analytical reagent, purity > 98%), 1.33 g Nb_2O_5 (analytical reagent, purity 99.9%) and 0.01 g CaCO_3 (analytical reagent, purity 99.9%) was mixed via ball milling in ethanol for 24 h. The mixed sample was heated in an oven to evaporate the ethanol, and the dry powder was acquired. The powder was calcined in a furnace at 1100 °C for 5 h to obtain pure phase LCNO powder. The NiO (analytical reagent, purity 99.8%) was added to the LCNO sample in two different ways. One was the external addition, and the other was the internal doping. To obtain 1 wt.% NiO-doped LCNO by an external addition method, the pure phase LCNO powder was mixed with NiO in a mass ratio of LCNO (100):NiO (1), and the dry powder was acquired by using the same ball milling method. For comparison, La_2O_3 , Nb_2O_5 , CaCO_3 , and NiO were used as starting powders to compose 1 wt.% NiO-doped LCNO powder internally. Ni partially replaced Nb in the lattice, and the amount of defect Nb_2O_5 was calculated according to the molar amount of the NiO. The powder was also calcined at 1100 °C for 5 h to obtain pure phase NiO-doped LCNO powder. The phase structures of the powders were identified by X-ray diffraction (XRD, with $\text{CuK}\alpha$ radiation, Ultima IV, Rigaku, Tokyo, Japan). The angle range is from 20° to 80°. The scanning rate is 3° per minute.

Both powders were pressed into pellets and sintered at 1400 °C for 5 h to densify the pellet for the conductivity tests. The morphologies of the sintered samples were observed by a field-emission scanning electron microscope (SEM, CHI760E, JEOL, Tokyo, Japan), and

the elemental distribution of the sintered membranes was analyzed by energy-dispersive X-ray spectroscopy (EDS, X-Max 50, Oxford Instruments, Oxford, UK).

The conductivity tests were carried out for the dense LCNO pellets that had been sintered at 1400 °C. To test the conductivity of the samples, both sides of sintered pellets were painted with silver paste, then the pellets were heated at 800 °C for 2 h to remove organics and form the silver electrodes for electrochemical testing. The pellets were tested in a fuel cell condition to explore the conductivity of the oxides under the fuel cell testing condition, using an electrochemical workstation (Admiral Plus, Admiral Instrument, Tempe, AZ, USA). The range of experiment temperatures is from 700 to 400 °C, and the conductivity was measured in 50 °C intervals. The single cells were tested with humidified hydrogen (~3% H₂O) as the fuel, with a flowing rate of 20 mL·min⁻¹ and static air as the oxidant. We used the four-probe method for the conductivity measurement, and it was measured by an impedance spectroscopy method. The fitting of the impedance was performed using the RelaxIS software (RelaxIS 3, rhd instruments GmbH & Co. KG, Darmstadt, Germany) with a model of two distributed elements composed of a constant phase element in parallel with a resistance. Theoretical calculations were carried out by using the VASP software (VASP 6.1.1, University of Vienna, Vienna, Austria), and the calculation details can be found in our previous studies [19–22].

3. Results and Discussion

3.1. Phase, Surface and Conductivity Comparisons of Different Doping LCNO

Figure 1 shows the X-ray diffraction (XRD) patterns of LCNO powder and 1 wt.% NiO-doped LCNO powders (externally and internally) after firing at 1100 °C. One can see that both doped powders are pure phases without any detectable secondary phases. The pure phase 1 wt.% NiO internally doped powder suggests that the material still has the original structure, and the doping of NiO does not change the material structure. However, it is interesting that 1 wt.% NiO externally doped powder is also free of any impurities. During powder synthesis, the NiO source was added externally to obtain a composite of LCNO and 1 wt.% NiO, which means that the NiO peak should be shown in the XRD pattern. The absence of the NiO peak is probably due to the very low amount of NiO used in the current case, which leads to undefined NiO peaks in the XRD pattern. By comparing the LCNO XRD with the standard LNO PDF card (22–1125), we find that this phase of the synthesized powders agrees well with the standard PDF card (22–1125) of LNO, suggesting that they are compounds instead of individual oxides. The peaks at 35, 38 and 57 reflect (200), (−211)/(112) and (−321) planes of the LNO, respectively. We can see there are no obvious extra peaks, suggesting that the materials are pure phase. The shapes of the peaks show some differences, which may result from the incorporation of NiO.

Figure 2 shows the surface of the LCNO and 1 wt.% NiO-doped LCNO (externally and internally) electrolyte membranes after sintering at 1400 °C for 5 h. One can see that all three of these pellets are dense and without noticeable pores, suggesting that 1400 °C is a sufficient temperature to densify the LCNO samples. However, despite the high density obtained for the NiO-free sample, its grain size is obviously smaller than that of the NiO-modified samples, indicating that the use of NiO as the dopant is helpful for the grain growth of LCNO, regardless of if the NiO is added externally or internally. Further comparing the external and internal strategies, the sample with the NiO added internally has a larger grain size compared with the sample with the NiO added externally. By using the line interception procedure, average grain sizes of LCNO and 1 wt.% NiO-doped LCNO (externally and internally) were calculated as 0.76, 1.26 and 1.61 μm, respectively. It is understood that the large grain size could reduce the volume of the grain boundaries [23] and thus decrease the grain boundary resistance and increase the total conductivity. Therefore, it is expected that the internally doped LCNO sample should have better conductivity.

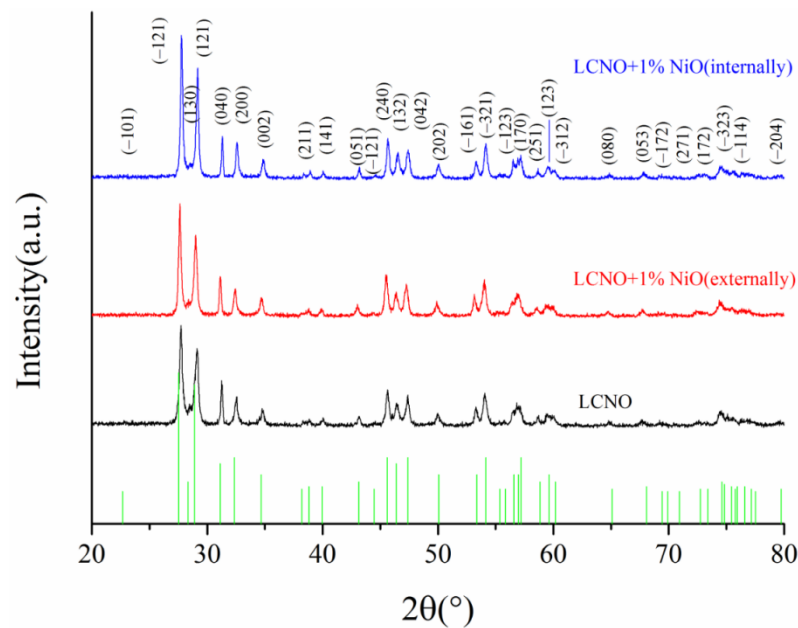


Figure 1. XRD patterns for LCNO powder and 1 wt.% NiO-doped LCNO powders (externally and internally) fired at 1100 °C.

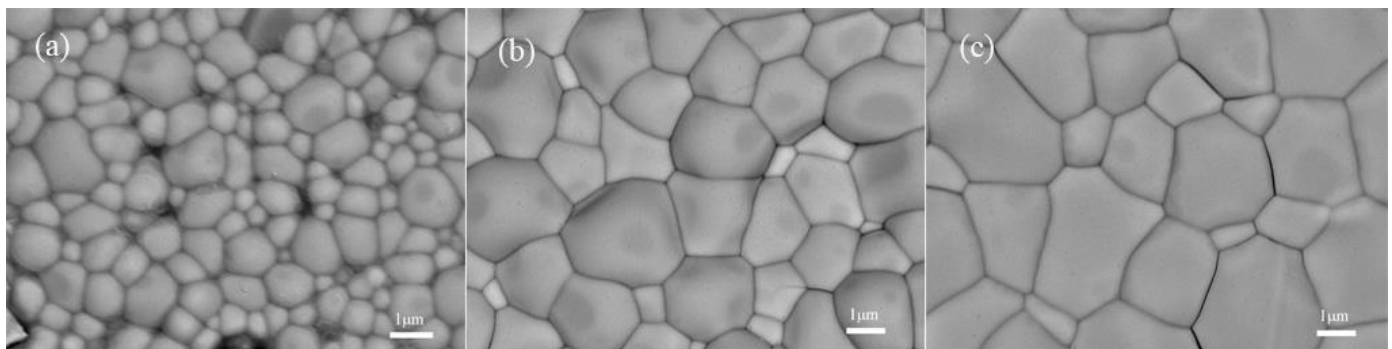


Figure 2. SEM images (shown in BSE) for the surface of (a) LCNO, (b) 1 wt.% NiO externally doped LCNO and (c) 1 wt.% NiO internally doped LCNO.

As shown in Figure 3, the electrical conductivity of internal doping over the entire temperature range is significantly higher than that of external doping and the LCNO pellet without NiO modification. The conductivity of the undoped LCNO, externally doped LCNO and internally doped LCNO is 0.45×10^{-3} , 0.98×10^{-3} and $1.16 \times 10^{-3} \text{ S}\cdot\text{cm}^{-1}$ at 700 °C, respectively. This result indicates that the strategy of using NiO as an internal dopant is superior to the traditional method of adding NiO externally.

It is evident that the strategy of using NiO internally can further improve the conductivity of LCNO compared with the traditional way of using NiO as the external sintering aid. Therefore, further explorations of the optimal content of NiO for LCNO were carried out. Figure 4a shows the X-ray diffraction (XRD) patterns of 1, 2 and 5 wt.% NiO-doped LCNO powders by an internal addition method after firing at 1100 °C. The pure phase was formed in 1 wt.% doping sample, and the XRD pattern for the 2 wt.% doping powder is almost the same as the 1 wt.% doping sample, which indicates that the sample also possesses the original structure. However, it is interesting that the 5 wt.% NiO-doped LCNO powder has extra peaks compared to 1 wt.% doping, suggesting this powder was not a pure phase and there were some other impurities. We hypothesize that the excessive peaks come from the NiO as the concentration of 5 wt.% NiO was too high to fully incorporate into the LCNO lattice. To confirm this, we compared the XRD pattern of pure phase

powder with that of the 5 wt.% doping sample and found that all extra peaks matched well with the peaks for NiO, and the result is shown in Figure 4b. Undoubtedly, 5 wt.% NiO-doped LCNO powder contains NiO as the impurity, while 1 and 2 wt.% NiO-doped LCNO powders are pure phase.

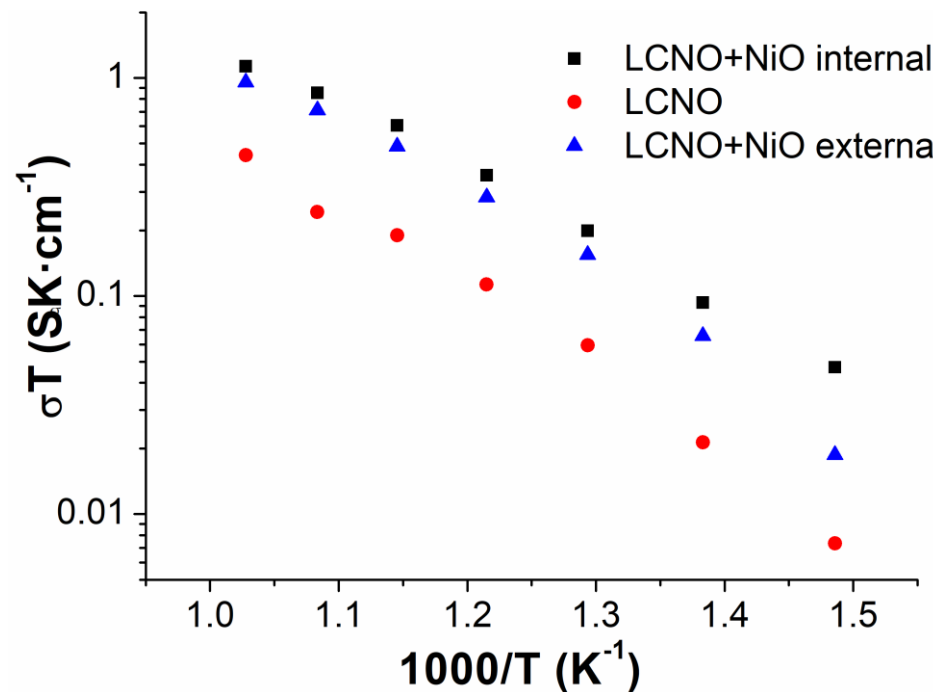


Figure 3. The conductivities of the LCNO pellet without NiO addition, and LCNO with 1 wt.% NiO addition externally and internally.

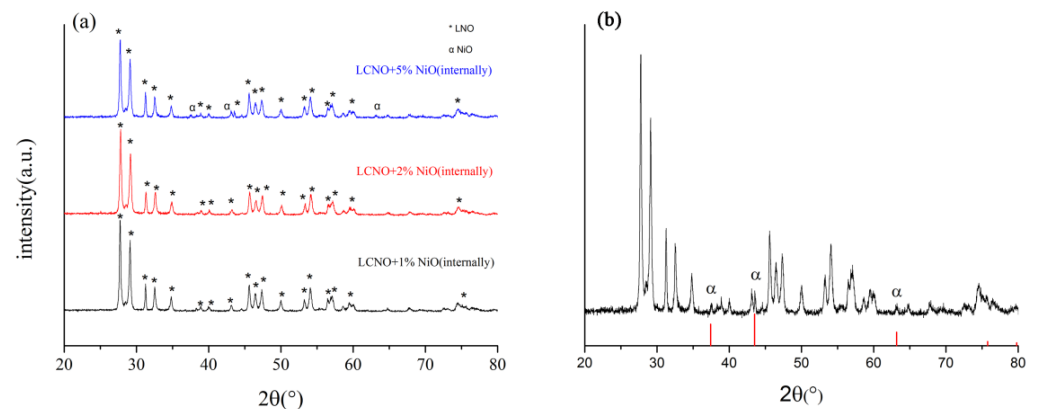


Figure 4. (a) XRD patterns for 1, 2 and 5 wt.% NiO-doped LCNO powders by an internal addition method fired at 1100 °C; (b) labels of excessive peaks from 5 wt.% doping XRD patterns.

Figure 5 shows the surface of 1, 2 and 5 wt.% NiO-doped LCNO electrolyte membranes after sintering at 1400 °C for 5 h. It can be observed that all three of these pellets are dense. However, there are some differences in the grain size of the pellets. The grain size of the 1 and 2 wt.% doped samples is similar, while that of the 5 wt.% doped sample is relatively smaller, which may be due to the extra NiO that inhibits the grain growth. By using the line interception procedure, the average grain sizes of 1, 2 and 5 wt.% NiO-doped LCNO were calculated as 1.61, 1.53 and 1.32 μm, respectively. There is a grain with a deep color in Figure 5c, which indicates that there is a Ni element accumulation in this place. We assume that this is due to the uneven distribution of NiO, which is confirmed in the SEM-EDS results.

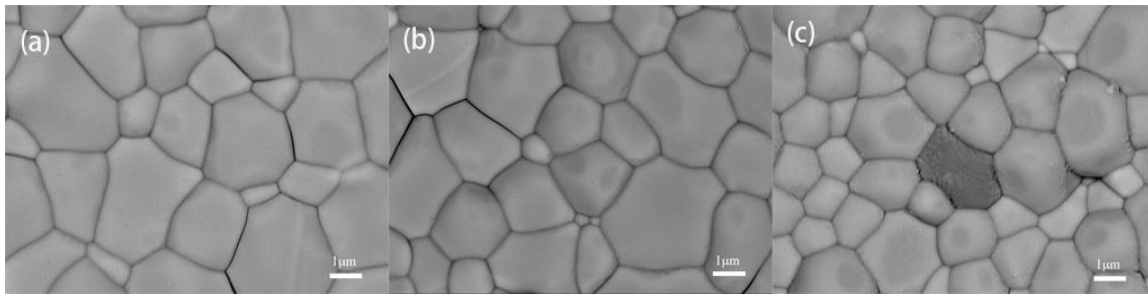


Figure 5. SEM images (shown in BSE) for the surface of (a) 1 wt.% NiO internally doped LCNO, (b) 2 wt.% NiO internally doped LCNO and (c) 5 wt.% NiO internally doped LCNO.

The elemental distribution of the samples was further analyzed by SEM-EDS. Figure 6 shows the SEM-EDS results for 1, 2 and 5 wt.% NiO-doped LCNO electrolyte membranes. The elemental analysis indicates that a relatively homogeneous Ni distribution is presented for 1 and 2 wt.% doped pellets. In contrast, it can be observed that the Ni element is unevenly distributed for 5 wt.% NiO-doped electrolyte, and an obvious accumulation of Ni element can be detected that agrees well with the XRD analysis. It would be reasonable to assume that the accumulation of NiO, as well as the smaller grain size, could deteriorate the conductivity of the sample.

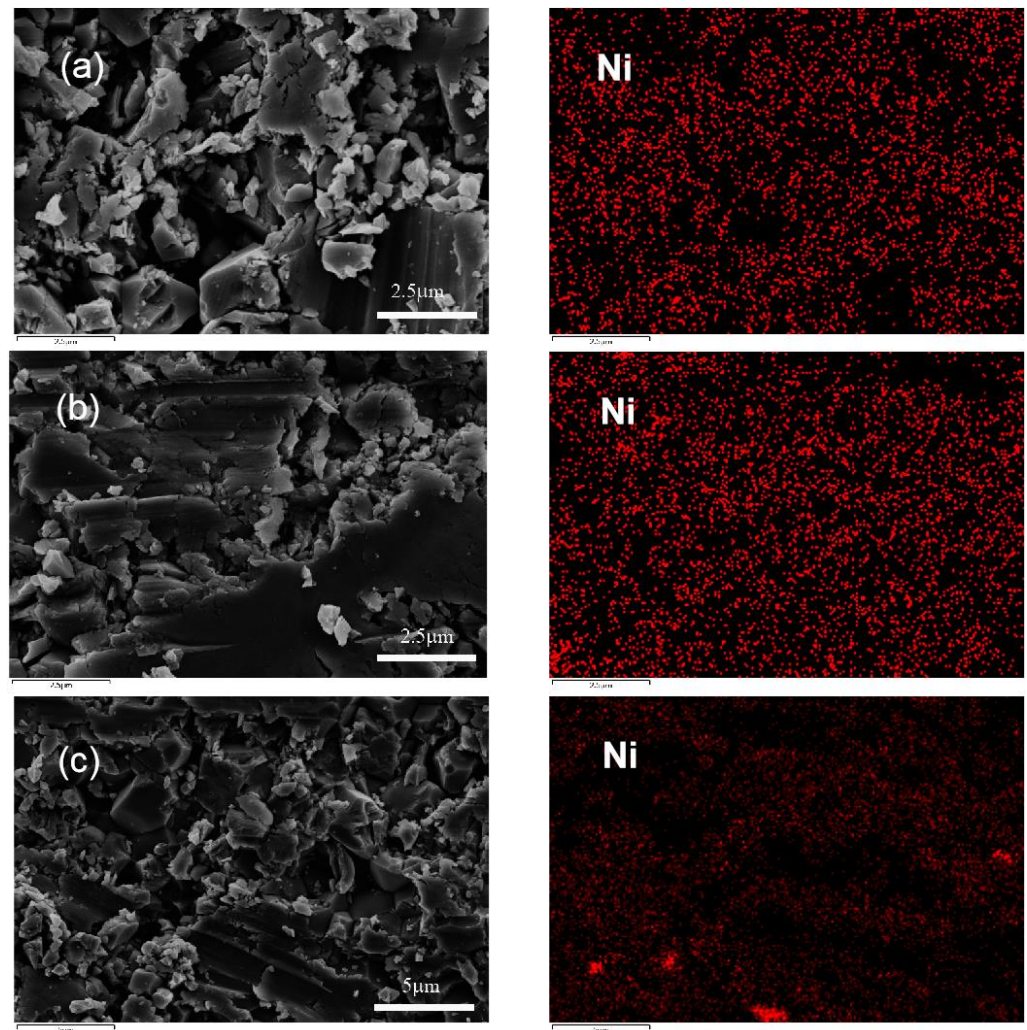


Figure 6. SEM-EDS mapping results for (a) 1 wt.% NiO internally doped LCNO, (b) 2 wt.% NiO internally doped LCNO and (c) 5 wt.% NiO internally doped LCNO.

Figure 7 shows the conductivity of 1, 2 and 5 wt.% NiO-doped LCNO electrolyte. One can see that the performances of 1 and 2 wt.% doping are relatively favorable, but the effect of 5 wt.% NiO on performance improvement is small. As shown in Figure 5, the grain sizes of 1 and 2 wt.% internal doping are slightly larger than that of 5 wt.%. Evidently, it could be easier for protons to transfer into samples with larger grain sizes, which reduce the grain boundary resistance. Additionally, compared to the first two samples, the element distribution of 5 wt.% doping is more uneven. Therefore, it can be concluded that 1 and 2 wt.% doping samples showed larger grain sizes and a more homogeneous distribution of elements. This may be why the performances of the first two samples are better than the 5 wt.% doped one. If we examine the conductivity difference between the 1 and 2% samples, they show similar conductivity at high temperatures, but the difference in conductivity increases at low temperatures. For instance, the conductivity for the 1, 2 and 5% doped sample is 1.16×10^{-3} , 1.25×10^{-3} and 0.49×10^{-3} S·cm⁻¹ at 700 °C, respectively. In contrast, the conductivity value at 400 °C is 7×10^{-5} , 3.1×10^{-5} and 1.1×10^{-5} S·cm⁻¹ for the 1%, 2% and 5% doped samples, respectively. The conductivity for the 1% sample is higher than that of the traditional LCNO reported in the literature that reaches around 1×10^{-3} S·cm⁻¹ at 800 °C [16]. The observed inflection point on the dependences both in Figures 3 and 7 may be a result of the phase transformation of the LCNO-based material, as reported in the literature [16]. The activation energy was calculated for the samples, indicating the activation energy of 0.62, 0.74 and 0.77 eV for 1%, 2% and 5% samples, respectively. The change in the activation energy may be related to the composition change that we elaborate on in the following section.

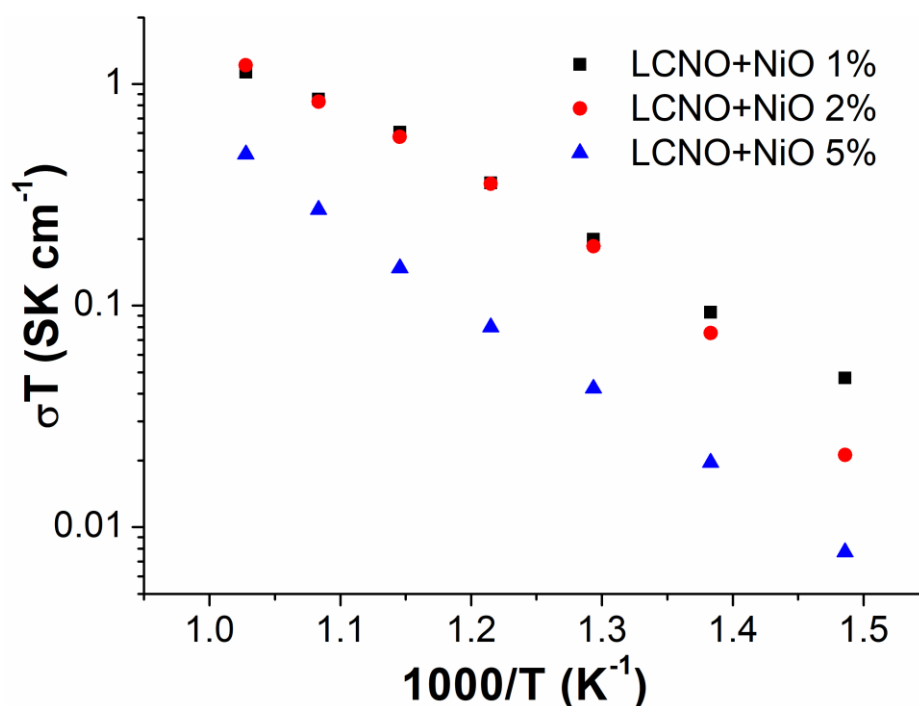


Figure 7. The conductivity of 1, 2 and 5 wt.% NiO-doped LCNO electrolyte.

The lattice parameters of pure LCNO; 1% external doping; and 1%, 2% and 5% internal doping samples were calculated as 332.884, 333.260, 332.782, 332.845, 333.167 Å³, respectively. Rietveld refined XRD patterns are also shown in Figure 8. The lattice volume would be expected to decrease if Ni replaced Nb and was completely doped into the lattice, as the ionic radius of Ni²⁺ (60 pm) is smaller than that of Nb⁵⁺ (64 pm) [24,25]. When the 1% is applied with the internal method, the expected decrease in lattice volume is observed. However, the lattice volume increases from 1% to 2%, although the lattice volume of the 2% sample is still smaller than that of the undoped LCNO, implying that Ni is not fully

incorporated into the lattice. The increase in lattice volume is more obvious prominent in the 5% doped sample and the sample with 1% NiO added externally (333.260 \AA^3), suggesting that the limitation in lattice solution could increase the lattice volume. Although no obvious accumulation of NiO can be observed in SEM and XRD for the 2% sample, likely due to the low concentration beyond the detection of the instruments, the change in the lattice volume suggests that the solubility limit for NiO-doped LCNO is between 1 and 2%. It seems that not all the 2% NiO is incorporated into the LCNO lattice, which might be the reason for the decreased conductivity at lower temperatures and higher activation energy compared with that of the 1% doped sample.

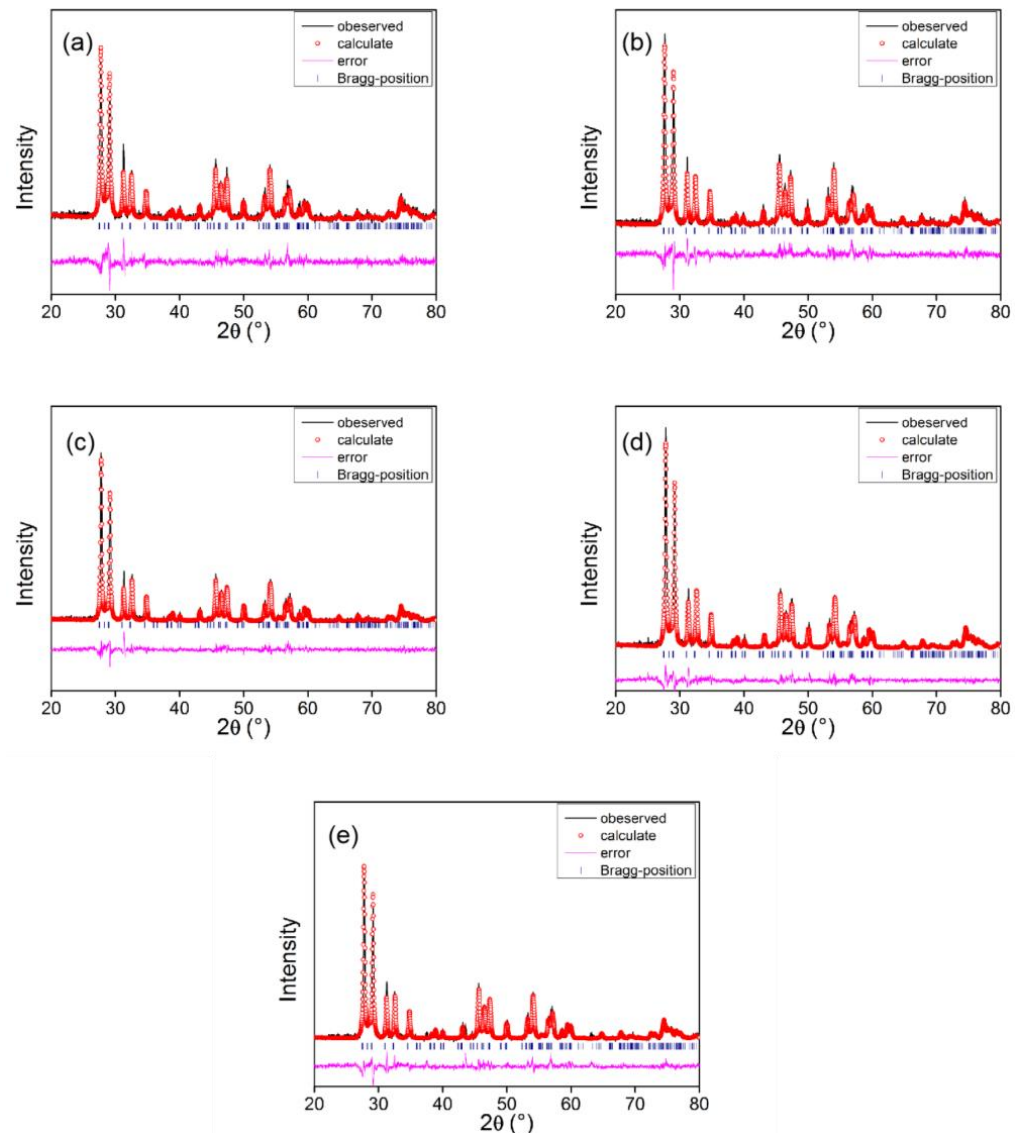


Figure 8. Rietveld refined XRD patterns of (a) undoped LCNO, (b) 1% externally doped LCNO, (c) 1% internally doped LCNO, (d) 2% internally doped LCNO and (e) 5% internally doped LCNO.

3.2. DFT

It is noted that the conductivity of the 1 and 2 wt.% NiO-doped LCNO shows higher conductivity than that of the LCNO pellets sintered at higher temperatures, as reported in the literature [16], implying that the tailoring of LCNO with NiO is an effective strategy to promote the protonation of LCNO. In order to prove this hypothesis, first-principle calculations were carried out. It is known that protonation happens when oxygen vacancies

are created, and proton defects are formed in the wet atmosphere according to the equation $\text{H}_2\text{O} + \text{V}_{\text{O}}^{\bullet\bullet} + \text{O}_{\text{O}}^{\times} \rightleftharpoons 2\text{OH}^{\bullet}$ [26].

Therefore, the oxygen vacancy formation energy (E_{V_O}) and the hydration energy ($E_{\text{hydration}}$) were calculated for LCNO with and without NiO modification. NiO was used internally as the dopant; therefore, NiO was incorporated into the lattice by replacing Nb atoms in the calculation. Figure 9 shows the optimized configuration of the LaNbO_4 with and without NiO modification by the DFT method, and one can see that the Ni atom partially occupies the Nb site for the NiO-modified sample. The oxygen vacancy formation energy (E_{V_O}) was calculated as 5.98 and 0.78 eV for the samples with and without the NiO modification, respectively. The result indicates that the introduction of NiO into the lattice can significantly lower the E_{V_O} , which is likely due to the low valence of Ni compared with the Nb. The replacement of Nb^{5+} by Ni^{2+} in the lattice could generate oxygen vacancies that, in principle, benefit the protonation (hydration) procedure. The calculated hydration energy ($E_{\text{hydration}}$) is -1.31 and -1.42 eV for the sample with and without the NiO modification, respectively. One can see that both values are negative, suggesting that hydration is thermodynamically favorable in both oxides. However, a more negative value was obtained when NiO was used, suggesting that NiO modification could have a better hydration ability than that of the NiO-free sample. Although there is no explanation as to why NiO is effective in improving the conductivity of LCNO, we can confirm that the replacement of Ni for Nb in the lattice could be beneficial for the oxygen vacancy formation as well as the hydration [27,28]. In addition, the replacement of Ni for Nb can form negative charges as $\text{Ni}_{\text{Nb}}^{''}$ in the lattice, which neutralizes the positive charge at the core of the space charge layer, thus mitigating the space charge layer effect and improving the conductivity accordingly [29]. Therefore, the improved conductivity of the NiO-modified LCNO is expected.

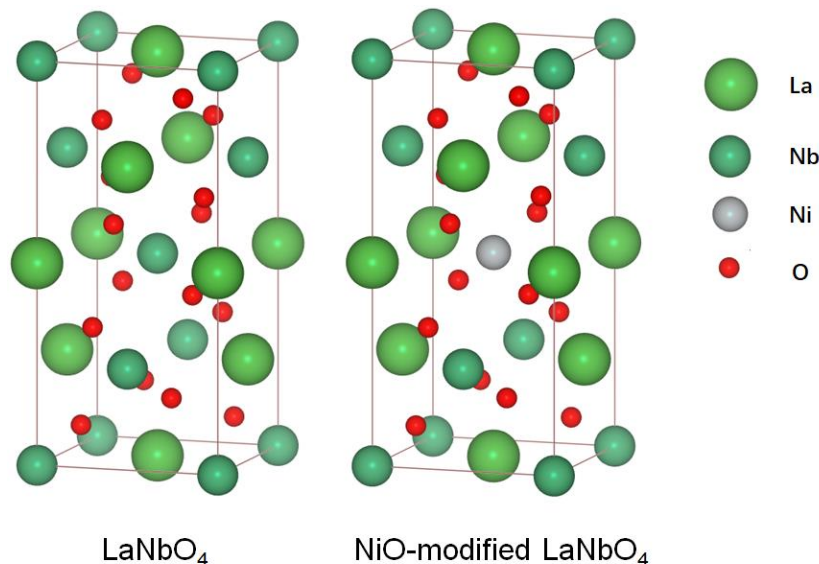


Figure 9. Configuration of LaNbO_4 - and NiO-modified LaNbO_4 optimized by the DFT method using the VASP software.

4. Conclusions

In this study, NiO was used as a sintering aid both internally and externally to explore the influence of NiO on the performance of the $\text{La}_{0.99}\text{Ca}_{0.01}\text{NbO}_4$ (LCNO) proton-conducting oxide. NiO has a significant impact on the grain growth of LCNO, regardless of if it is used internally or externally. However, the internal doping strategy shows an advantage in both conductivity and grain growth over that of the external strategy. Furthermore, the doping concentration has an evident impact on the performance of LCNO even within the internally doped samples. The sample shows good conductivity when the

doping concentration is low, and the conductivity decreases with the high NiO-doping concentration, which is due to the presence of the second phase and the accumulation of NiO. DFT calculations show that the doping of NiO into LCNO could lower the oxygen vacancy formation energy and the protonation (hydration) energy, facilitating the formation of protons and thus improving the conductivity.

Author Contributions: Investigation, K.Y. and X.L.; supervision, L.B.; writing—original draft, K.Y.; writing—review & editing, L.B. All authors have read and agreed to the published version of the manuscript.

Funding: This work was supported by the Key Research and Development Program of Shandong Province (Grant No.: 2019GGX103020).

Institutional Review Board Statement: Not applicable.

Informed Consent Statement: Not applicable.

Data Availability Statement: Data is contained within the article. The data presented in this study are available in article.

Conflicts of Interest: The authors declare no conflict of interest.

References

1. Wachsman, E.D.; Lee, K.T. Lowering the temperature of solid oxide fuel cells. *Science* **2011**, *334*, 935–939. [[CrossRef](#)] [[PubMed](#)]
2. Dai, H.; Kou, H.; Wang, H.; Bi, L. Electrochemical performance of protonic ceramic fuel cells with stable BaZrO₃-based electrolyte: A mini-review. *Electrochem. Commun.* **2018**, *96*, 11–15. [[CrossRef](#)]
3. Wachsman, E.; Ishihara, T.; Kilner, J. Low-temperature solid-oxide fuel cells. *MRS Bull.* **2014**, *39*, 773–779. [[CrossRef](#)]
4. Tang, H.; Jin, Z.; Wu, Y.; Liu, W.; Bi, L. Cobalt-free nanofiber cathodes for proton conducting solid oxide fuel cells. *Electrochem. Commun.* **2019**, *100*, 108–112. [[CrossRef](#)]
5. Xia, Y.; Jin, Z.; Wang, H.; Gong, Z.; Lv, H.; Peng, R.; Liu, W.; Bi, L. A novel cobalt-free cathode with triple-conduction for proton-conducting solid oxide fuel cells with unprecedented performance. *J. Mater. Chem. A* **2019**, *7*, 16136–16148. [[CrossRef](#)]
6. Duan, C.C.; Tong, J.H.; Shang, M.; Nikodemski, S.; Sanders, M.; Ricote, S.; Almansoori, A.; O’Hayre, R. Readily processed protonic ceramic fuel cells with high performance at low temperatures. *Science* **2015**, *349*, 1321–1326. [[CrossRef](#)]
7. Han, D.; Shinoda, K.; Sato, S.; Majima, M.; Uda, T. Correlation between electroconductive and structural properties of proton conductive acceptor-doped barium zirconate. *J. Mater. Chem. A* **2014**, *3*, 1243–1250. [[CrossRef](#)]
8. Tarutin, A.P.; Lyagaeva, J.G.; Medvedev, D.A.; Bi, L.; Yaremchenko, A.A. Recent advances in layered Ln₂NiO_{4+δ} nickelates: Fundamentals and prospects of their applications in protonic ceramic fuel and electrolysis cells. *J. Mater. Chem. A* **2021**, *9*, 154–195. [[CrossRef](#)]
9. Bi, L.; Boulfrad, S.; Traversa, E. Steam electrolysis by solid oxide electrolysis cells (SOECs) with proton-conducting oxides. *Chem. Soc. Rev.* **2014**, *43*, 8255–8270. [[CrossRef](#)]
10. Medvedev, D.A.; Lyagaeva, J.G.; Gorbova, E.V.; Demin, A.K.; Tsiakaras, P. Advanced materials for SOFC application: Strategies for the development of highly conductive and stable solid oxide proton electrolytes. *Prog. Mater. Sci.* **2016**, *75*, 38–79. [[CrossRef](#)]
11. Li, J.; Wang, C.; Wang, X.; Bi, L. Sintering aids for proton-conducting oxides—A double-edged sword? A mini review. *Electrochem. Commun.* **2020**, *112*, 106672. [[CrossRef](#)]
12. Haugrud, R.; Norby, T. High-temperature proton conductivity in acceptor-substituted rare-earth ortho-tantalates, LnTaO₄. *J. Am. Ceram. Soc.* **2007**, *90*, 1116–1121. [[CrossRef](#)]
13. Fjeld, H.; Kepaptsoglou, D.M.; Haugrud, R.; Norby, T. Charge carriers in grain boundaries of 0.5% Sr-doped LaNbO₄. *Solid State Ion.* **2010**, *181*, 104–109. [[CrossRef](#)]
14. Magraso, A.; Fontaine, M.L.; Larring, Y.; Bredesen, R.; Syvertsen, G.E.; Lein, H.L.; Grande, T.; Huse, M.; Strandbakke, R.; Haugrud, R.; et al. Development of proton conducting SOFCs based on LaNbO₄ electrolyte—status in Norway. *Fuel Cells* **2011**, *11*, 17–25. [[CrossRef](#)]
15. Bi, L.; Fabbri, E.; Traversa, E. Solid oxide fuel cells with proton-conducting La_{0.99}Ca_{0.01}NbO₄ electrolyte. *Electrochim. Acta* **2018**, *260*, 748–754. [[CrossRef](#)]
16. Haugrud, R.; Norby, T. Proton conduction in rare-earth ortho-niobates and ortho-tantalates. *Nat. Mater.* **2006**, *5*, 193–196. [[CrossRef](#)]
17. Haile, S.M.; Staneff, G.; Ryu, K.H. Non-stoichiometry, grain boundary transport and chemical stability of proton conducting perovskites. *J. Mater. Sci.* **2001**, *36*, 1149–1160. [[CrossRef](#)]
18. Peng, C.; Melnik, J.; Luo, J.L.; Sanger, A.R.; Chuang, K.T. BaZr_{0.8}Y_{0.2}O₃-delta electrolyte with and without ZnO sintering aid: Preparation and characterization. *Solid State Ion.* **2010**, *181*, 1372–1377. [[CrossRef](#)]
19. Ma, J.; Tao, Z.; Kou, H.; Fronzi, M.; Bi, L. Evaluating the effect of Pr-doping on the performance of strontium-doped lanthanum ferrite cathodes for protonic SOFCs. *Ceram. Int.* **2020**, *46*, 4000–4005. [[CrossRef](#)]

20. Xu, X.; Wang, H.; Ma, J.; Liu, W.; Wang, X.; Fronzi, M.; Bi, L. Impressive performance of proton-conducting solid oxide fuel cells using a first-generation cathode with tailored cations. *J. Mater. Chem. A* **2019**, *7*, 18792–18798. [[CrossRef](#)]
21. Xu, X.; Wang, H.; Fronzi, M.; Wang, X.; Bi, L.; Traversa, E. Tailoring cations in a perovskite cathode for proton-conducting solid oxide fuel cells with high performance. *J. Mater. Chem. A* **2019**, *7*, 20624–20632. [[CrossRef](#)]
22. Ji, Q.Q.; Xu, X.; Liu, X.H.; Bi, L. Improvement of the catalytic properties of porous lanthanum manganite for the oxygen reduction reaction by partial substitution of strontium for lanthanum. *Electrochem. Commun.* **2021**, *124*, 1873–1902. [[CrossRef](#)]
23. Fabbri, E.; Bi, L.; Tanaka, H.; Pergolesi, D.; Traversa, E. Chemically stable Pr and Y Co-doped barium zirconate electrolytes with high proton conductivity for intermediate-temperature solid oxide fuel cells. *Adv. Funct. Mater.* **2010**, *21*, 158–166. [[CrossRef](#)]
24. Zhang, C.; Wang, Y.; Li, G.; Chen, L.; Zhang, Q.; Wang, D.; Li, X.; Wang, Z. Tuning smaller Co₃O₄ nanoparticles onto HZSM-5 zeolite via complexing agents for boosting toluene oxidation performance. *Appl. Surf. Sci.* **2020**, *532*, 147320. [[CrossRef](#)]
25. Zeng, K.; Wang, Y.; Huang, C.; Liu, H.; Liu, X.; Wang, Z.; Yu, J.; Zhang, C. Catalytic combustion of propane over MnNbO_x composite oxides: The promotional role of niobium. *Ind. Eng. Chem. Res.* **2021**, *60*, 6111–6120. [[CrossRef](#)]
26. Kreuer, K. Proton-conducting oxides. *Annu. Rev. Mater. Res.* **2003**, *33*, 333–359. [[CrossRef](#)]
27. Xu, Y.S.; Liu, X.H.; Cao, N.; Xu, X.; Bi, L. Defect engineering for electrocatalytic nitrogen reduction reaction at ambient conditions. *Sustain. Mater. Technol.* **2021**, *27*, e00229.
28. Xu, Y.S.; Xu, X.; Cao, N.; Wang, X.F.; Liu, X.H.; Fronzi, M.; Bi, L. Perovskite ceramic oxide as an efficient electrocatalyst for nitrogen fixation. *Int. J. Hydrogen. Energ.* **2021**, *46*, 10293–10302. [[CrossRef](#)]
29. Shirpour, M.; Rahmati, B.; Sigle, W.; van Aken, P.A.; Merkle, R.; Maier, J. Dopant segregation and space charge effects in proton-conducting BaZrO₃ perovskites. *J. Phys. Chem. C* **2012**, *116*, 2453–2461. [[CrossRef](#)]